Science of Sintering, **53** (2021) 55-66

https://doi.org/10.2298/SOS2101055D

UDK: 546.87; 546.881.4; 532.74

Fast Oxide-Ion Conductors in Bi_2O_3-V_2O_5 System: $Bi_{108-x}V_xO_{162+x\,(x\,=\,4-9)}$ with 3 × 3 × 3 Superstructure

A. Dapčević[1*)], A. Radojković[2], M. Žunić[2], M. Počuča-Nešić[2], O. Milošević[2], G. Branković[2]

[1]University of Belgrade, Department of General and Inorganic Chemistry, Faculty of Technology and Metallurgy, Karnegijeva 4, 11000 Belgrade, Serbia

[2]University of Belgrade, Institute for Multidisciplinary Research, Kneza Višeslava 1a, 11000 Belgrade, Serbia

Abstract:

In this study, the possibility to stabilize O^{2-} ion conductors in Bi_2O_3-V_2O_5 system was investigated. Six pseudo-binary Bi_2O_3-V_2O_5 mixtures [3.50 < x(V_2O_5) < 8.50 mol%] were thermally treated at 1000 °C for 1 h. The samples were characterized by XRD, HRTEM/SAED, DTA and EIS techniques. The high-temperature reaction between α Bi_2O_3 and V_2O_5 resulted in formation of microcrystalline single-phase specimens containing the phase based on δ-Bi_2O_3 if V_2O_5 content was ≥ 4.63 mol%. The obtained phases exhibited main diffraction peaks corresponding to the simple cubic δ-Bi_2O_3 (space group Fm-3m) but Rietveld refinement showed a threefold repeat on a simple cubic sublattice indicating that the true unit cell is 3×3×3 supercell. Within proposed supercell, the octahedrally coordinated V^{5+} ions fully occupy 4a Wyckoff position and partially occupy 32f. The Bi^{3+} ions are placed at the rest of 32f and at 24e and 48h with full occupation. In total, 22 % of anionic sites are vacant. The ionic conductivity of phase with the lowest dopant content, i.e. $Bi_{103}V_5O_{167}$, amounts 0.283 S cm^{-1} at 800 °C with the activation energy of 0.64(5) eV, which is comparable to the undoped δ-Bi_2O_3 known as the fastest ion conductor.

Keywords: *Bi_2O_3; V_2O_5; Ion conductors; Supercell.*

1. Introduction

The demand for new environmental-friendly technologies for energy production increases the interest in electrolytes based on oxide ion conductors because of their application in solid oxide fuel cells (SOFCs) *whose development and widespread use might become a keystone in the near future* [1-4]. In general, the oxide ion conducting materials should possess highly symmetric structure with significant number of oxygen vacancies [5] as it is the case with commercially used yttria stabilized zirconia (YSZ), *i. e.* the ZrO_2 crystallizes in a cubic structure having oxygen vacancies provided by Y_2O_3 [6] and cubic gadolinium-doped ceria (GDC) [7] in which the substitution of 10-20 % of Ce^{4+} by Gd^{3+} generates enough oxygen vacancies in the lattice for optimal ionic conductivity [8]. The greatest disadvantage of YSZ is its very high operating temperature (about 1000 °C) [9, 10] while GDC is sensitive to reducing conditions and possesses undesirable electronic conductivity [11]. As a solution, Wachsman and Lee [12] have proposed a bilayer electrolyte, which consists of GDC layer on the anode side and erbia stabilized δ-Bi_2O_3 on the cathode

*) **Corresponding author:** hadzi-tonic@tmf.bg.ac.rs

side. In this way, the stability of electrolyte could be preserved. The δ-Bi_2O_3 polymorph demonstrates one of the highest conductivity, which are one to two orders of magnitude higher than that of YSZ or GDC at corresponding temperatures [12]. This is the consequence of highly symmetric pseudo-fluorite structure in which 25 % of oxygen sites are vacant. Besides, Bi^{3+} ions possess the $6s^2$ lone electron pair, providing a highly polarizable cation network that facilitates higher anion mobility.

However, there are still a lot of controversies about this structure. At the beginning, it was considered as a simple cubic pseudo-fluorite structure. In 1937, Sillén [13] was first to propose a structural model according to which δ-Bi_2O_3 phase crystallizes in $Pn\bar{3}m$ space group [a = 5.525(5) Å] with the oxygen vacancies ordered along <111>. A similar atom arrangement and cubic symmetry were also suggested by Gattow and Schröder [14] 25 years later. According to this model, δ-Bi_2O_3 phase crystallizes in $Fm\bar{3}m$ space group [a =5.665(8) Å] with Bi atoms located at 4a site with disordered oxygen sublattice, in which the vacancies randomly take 25 % of available 8c sites. None of these models can account this particularly high ionic conductivity, which could be only associated with the disordered state comparable to 75 % of the liquid state [15]. Harwig [16] and Willis [17] suggested the moving of O^{2-} ions from tetrahedral 8c to octahedral 32f sites, which results in an occupancy factor of 3/16. Battle [18] and Yashima and Ishimura [19] proposed a random distribution of O^{2-} ions over these two positions with a partial averaged occupancy.

The δ-Bi_2O_3 phase is however a high-temperature polymorph, unstable upon cooling. Namely, on heating the stable low-temperature polymorph α-Bi_2O_3 transforms to δ-Bi_2O_3 phase at 730 °C, which melts at about 825 °C. On cooling two transitions are possible: δ-Bi_2O_3 → β-Bi_2O_3 at 650 °C or δ-Bi_2O_3 → γ-Bi_2O_3 at 640 °C, dependently of dopant [16, 20]. Still, the cubic δ-Bi_2O_3 phase can be stabilized down to the room temperature by doping with elements of group 5 (V, Nb, Ta) and some lanthanides [1, 21] which is regularly accompanied with the decreasing of conductivity. The doping complicates the crystal structure determination even more because the additional ordering between cationic positions of bismuth and dopant is expected together with the mentioned vacancy ordering. As a consequence, the modulated structures based on pseudo-fluorite structure could be formed.

Boyapati *et al.* [22, 23] reported the difference in δ-Bi_2O_3 structure at higher and lower temperatures due to different vacancy arrangements as a consequence of doping. The so-called order-disorder transition occurs at 600 °C. While the short-range vacancy ordering along <111> in domain-like way is characteristic for disordered structures, the long-range vacancy ordering along same directions exists in ordered structures and is followed by the displacement of almost all the oxygen ions from the regular 8c to the interstitial 32f positions. The authors describe the disordered structure in terms of combination of Gattow/Schröder [14] and Willis [17] models, whereas the ordered structures with a mixed Sillén-Willis model [13, 17]. Aidhy *et al.* [24] even reported the combination of vacancy ordering along <110> and <111>, which leads to a doubling of the unit cell that results in a $2 \times 2 \times 2$ fluorite supercell accompanied with symmetry lowering from $Fm\bar{3}m$ to $Fm\bar{3}$ space group.

In order to obtain a highly conductive material, a lot of authors were investigating the Bi_2O_3–V_2O_5 system. Based on microscopic experiments, Zhou [25, 26] divided possible superstructures within Bi_2O_3–V_2O_5 system into types: I (cubic 3×3×3) if 6.67 < V_2O_5 mol% ≤ 10, II (triclinic) if 10 < V_2O_5 mol% ≤ 25, III (tetragonal) if 25 < V_2O_5 mol% < 50, and IV (Aurivillius phases) for 50 mol% of V_2O_5. For the simplest type I, cubic 3×3×3 superstructure has been built up for $Bi_{100}V_8O_{170}$ composition because the V-atoms could be completely isolated from each other. With higher V_2O_5 content, it is not possible to separate all V atoms by at least one Bi atom and thus V_4O_{10} clusters are formed on the (111) plane of each cubic subcell within type II. The superstructure of type III is a hybrid of fluorite and pyrochlore structure. As mentioned, the Aurivillius phases and hence BIMEVOX (bismuth metal vanadium oxide) [27–29] compounds belong to the type IV. Other superstructures reported in

the literature mainly consider higher V_2O_5 concentration: triclinic for 14.8 [30] and 25.5 [31], monoclinic for 7.4 [32], 14.8 [33, 34] and 20.2 [35], orthorhombic for 11.6 and 33.0 [35], tetragonal for 15 [36], and hexagonal for 10 [37] mol% of V_2O_5.

In this study, the thermal treatment of six pseudo-binary Bi_2O_3-V_2O_5 mixtures in Bi_2O_3-rich region [$3.5 < x(V_2O_5) < 8.5$ mol%] were investigated in order to find a minimal V concentration that stabilizes δ-Bi_2O_3 phase down to room temperature giving a highly conductive material that could be used as a functional electrolyte for SOFCs. Moreover, a new structural model for V-doped δ-Bi_2O_3 is proposed with the aim to finally clarify the nature of this superstructure.

2. Materials and Experimental Procedures

Six stoichiometrically different mixtures (Table I) of α-Bi_2O_3 (Alfa Aesar, 99.975 %) and V_2O_5 (Aldrich, 99.9 %) were dry homogenized by hand-grinding for about 30 min in an agate mortar, heated at 1000 °C for 3 h (heating rate 4 °C min^{-1}) in an open Pt crucible and then furnace cooled to room temperature. The obtained samples were examined on an Ital Structure APD 2000 X-ray powder diffractometer using Cu $K\alpha$ radiation (λ = 1.5418 Å) and step-scan mode (2θ = 20–70 °). The unit cell parameters were calculated by least-squares method using the LSUCRIPC software [38]. The ICSD database was used for the phase identification [39].

Specifically, X-ray powder diffraction data of $Bi_{102}V_6O_{168}$ were collected in a range 4 – 125° 2θ with a step-width of 0.02° and a constant counting time of 7.5 s per step. The FULLPROF software was used for the Rietveld refinement [40] in WINPLOTR environment [41]. The profiles were described by the pseudo-Voigt function as the most frequently used function in this type of analysis [42, 43] with n in n×FWHM equal to 30 and limit for the peak asymmetry set to 90° 2θ. In the first stage of the refinement, the background was modeled by using a linear interpolation between 77 selected points and in the last cycles the Fourier filtering method with the window size set to 8000 was used. In final cycles of the refinement, a total of 21 parameters were refined using 6050 data points and 502 reflections. The site occupation factors were not refined. During the refinement of isotropic atomic displacement parameters (B_{iso}) of V and O atoms either nonpositive values were observed or the refinement became unstable. This can be explained by a great difference of Bi X-ray scattering powers compared to light V and O atoms. To avoid this problem, B_{iso} for light atoms were fixed to the values obtained within their individual refinement.

The cyclic differential thermal analysis (DTA) of the products was performed on an SDT Q600 instrument (TA Instruments) in N_2 atmosphere (flow rate: 100 cm^3 min^{-1}; heating rate: 20 °Cmin^{-1}), ranging from room temperature to 1000 °C. The powders were also investigated using a FEI TECNAI G2 F20 FE high resolution transmission electron microscope (HRTEM). To obtain dense (obtained densities exceeded 90 %) disk-shaped pellets for the electrochemical measurements, the powders were first uniaxially pressed under pressure of 200 MPa and then sintered at 800 °C for 3 h. The sintered pellets (prepared by applying Au paste on both sides followed by thermal treatment: 100 °C for 2 h and 750 °C for 30 min) were characterized by electrochemical impedance spectroscopy (EIS) using a HIOKI 3532-50 LCR HiTESTER in a frequency range 42 Hz-1 MHz and temperatures between 750 and 800 °C. The impedance spectra were fitted by EIS Spectrum Analyzer Software [44].

3. Results and Discussion

As shown in Table I, if V_2O_5 content was ≥ 4.63 mol% the high-temperature reaction between α-Bi_2O_3 and V_2O_5 resulted in formation of microcrystalline specimens containing a

phase based on δ-Bi_2O_3, which is denoted as δ*-Bi_2O_3. The only composition that did not lead to single-phase sample was the one with the lowest dopant content, $Bi_{104}V_4O_{166}$. If we take into account the initial composition of this mixture and its final phase composition, then the minimum dopant content necessary to stabilize the δ-Bi_2O_3 can be calculated giving 4.24 mol% of V_2O_5. As mentioned in the introduction, from the conductivity point of view, the maximum dopant content is not important and hence was not determined in this research but according to the Bi_2O_3–V_2O_5 phase diagram [45], it amounts 12.1 mol% of V_2O_5.

Tab. I Characteristics of prepared microcrystalline samples.

Starting composition	V_2O_5 content (mol%)	Phase composition (wt.%)	Unit cell parameters of obtained phases (Å/°)
$Bi_{104}V_4O_{166}$	3.70	δ*-Bi_2O_3 (84) + α-Bi_2O_3 (16)	$a_{\delta*}$ = 16.6579(3) a_α = 5.866(5) b_α = 8.199(6) c_α = 7.536(7) β_α = 112.91(7)
$Bi_{103}V_5O_{167}$	4.63	δ*-Bi_2O_3	$a_{\delta*}$ = 16.6651(4)
$Bi_{102}V_6O_{168}$	5.55	δ*-Bi_2O_3	$a_{\delta*}$ = 16.6522(4)
$Bi_{101}V_7O_{169}$	6.48	δ*-Bi_2O_3	$a_{\delta*}$ = 16.6367(2)
$Bi_{100}V_8O_{170}$	7.40	δ*-Bi_2O_3	$a_{\delta*}$ = 16.6327(3)
$Bi_{99}V_9O_{171}$	8.33	δ*-Bi_2O_3	$a_{\delta*}$ = 16.6325(2)

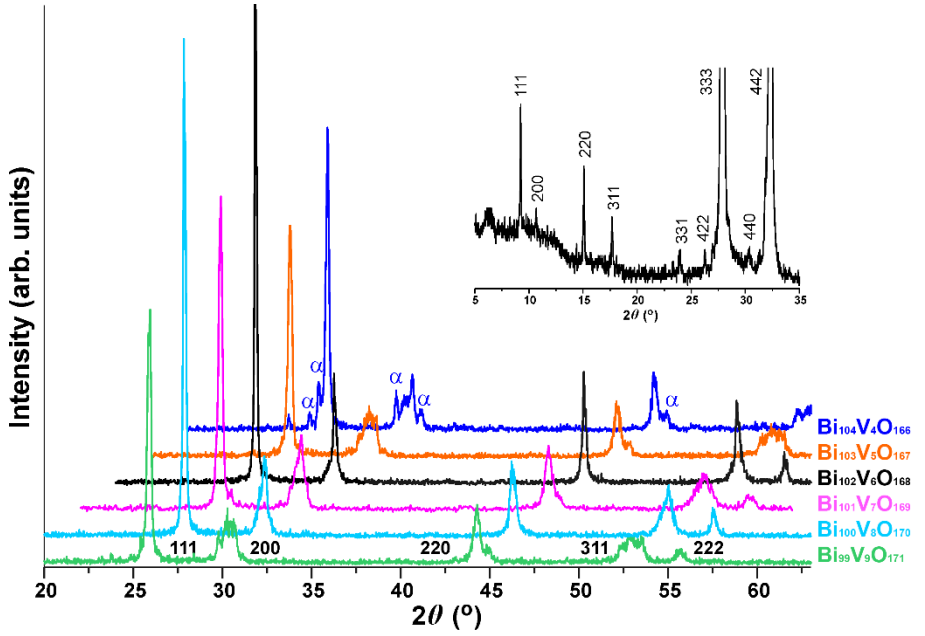

Fig. 1. XRD patterns of microcrystalline samples. The strong reflections are indexed for simple cubic pseudo-fluorite cell. The symbol α is used to denote the peaks of α-Bi_2O_3 phase. Inset: the enlarged part of $Bi_{102}V_6O_{168}$ XRD pattern with reflections indexed in 3×3×3 supercell based on cubic pseudo-fluorite subcell.

The obtained δ*-Bi_2O_3 phases show main diffraction peaks (Fig. 1) corresponding to the cubic δ-Bi_2O_3 (space group $Fm\bar{3}m$ and $a \approx 5.6$ Å). However, the detected weak reflections indicate a threefold repeat on a simple cubic sublattice saying that the true unit cell could be 3×3×3 supercell with $a \approx 16.6$ Å. According to Zhou's type I, the cubic 3×3×3 superstructure could be built up for $Bi_{100}V_8O_{170}$ composition, *i.e.* 108 cationic sites. So we presented the composition of obtained phases in that sense. The obvious decreasing of *a*-parameters with the dopant amount increasing is the consequence of smaller dopant ionic radius {$r_i(V^{5+}) = 0.54$ Å and $r_i(Bi^{3+}) = 1.03$ Å in the six-coordinated environment [46]}.

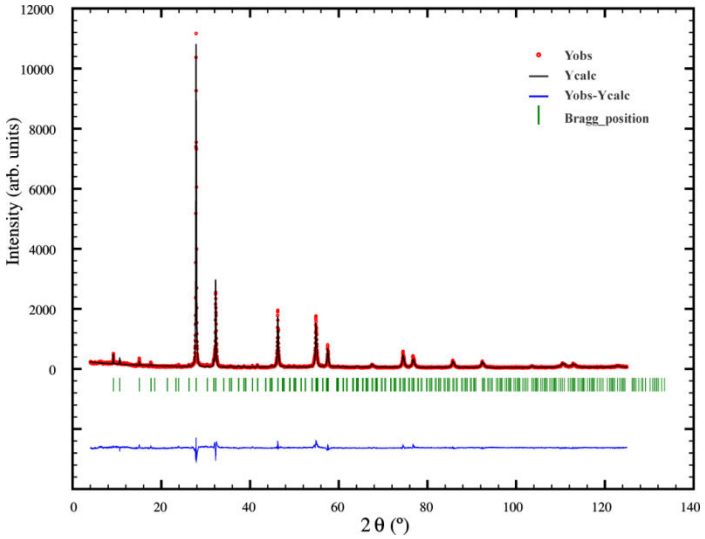

Fig. 2. The observed, calculated and difference profiles for the Rietveld refinement of $Bi_{102}V_6O_{168}$.

Tab. II Structural parameters for $Bi_{102}V_6O_{168}$.

$Bi_{102}V_6O_{168}$ space group: $Fm\bar{3}m$						
Atoms	Wyckoff position	*x*	*y*	*z*	*B* (Å^2)	normalized occupation
V1	4*a*	0	0	0	2	1
Bi1	24*e*	0.3290(5)	0	0	2.7(4)	1
Bi2/V2	32*f*	0.3371(2)	0.3371(2)	0.3371(2)	2.1(2)	1 (30/2)
Bi3	48*h*	0	0.1731(3)	0.1731(3)	3.1(2)	1
O1	24*e*	0.895(6)	0	0	1	1
O2	96*k*	0.361(2)	0.361(2)	0.207(3)	2	0.75
O3	96*k*	0.148(2)	0.148(2)	0.437(3)	2	0.75
R_{wp}=17.9% R_p=13.6% R_{exp}=9.08%						

The fact that δ*-Bi_2O_3 phases crystallize in 3×3×3 supercell and space group $Fm\bar{3}m$ is in agreement with the research of Zhou [25, 26]. Since we have obtained 3×3×3 modulated

phases for 4.63 ≤ V_2O_5 mol% ≤ 8.33, Zhou's type I could be assigned to here obtained phases with the interval of V_2O_5 concentration slightly extended to lower concentrations. In order to check the assumed superstructure, the $Bi_{102}V_6O_{168}$ sample was chosen for the Rietveld refinement (Fig. 2, Table II) because this sample showed the least visible weak reflections in the XRD pattern. The number of oxygen vacancies in $Bi_{102}V_6O_{168}$ (48 which is 22 %) is slightly lower comparing to the simple undoped δ-Bi_2O_3 (25 % of anionic sites are vacant) because of the partial replacement of trivalent Bi by pentavalent V.

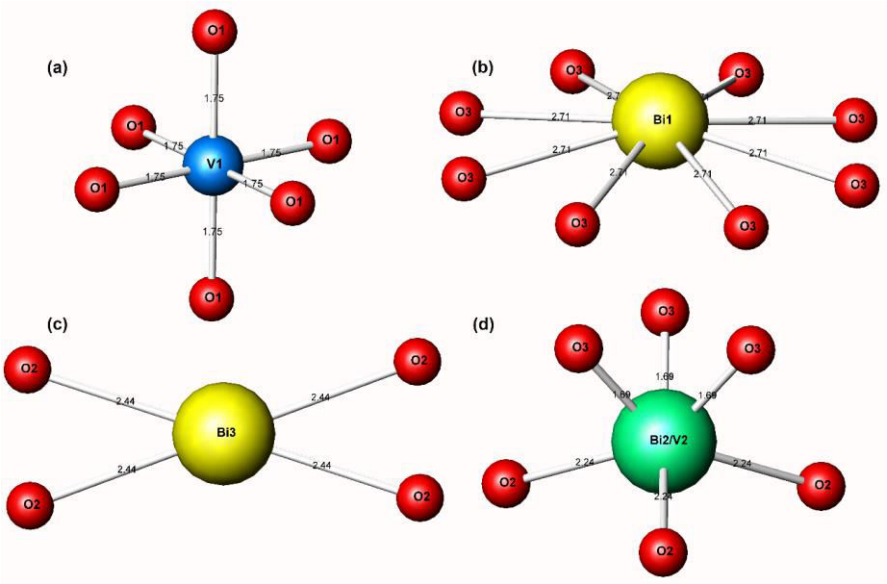

Fig. 3. The geometry of cations at 4*a* (a), 24*e* (b), 48h (c) and 32*f* (d) sites.

Within here proposed supercell, the octahedrally coordinated V^{5+} ions (Fig. 3a) fully occupy 4*a* Wyckoff position, *i.e.* the corners and face centers of cubic supercell, and partially occupy 32*f*. The Bi^{3+} ions are placed at the rest of 32*f* and at 24*e* and 48*h* with full occupation. At 24*e*, 32*f* and 48*h* site, the cations are eight (Fig. 3b), six (Fig. 3c) and four (Fig. 3d) coordinated, respectively. The space required for Bi lone electron pair is visible for all proposed coordinations of Bi^{3+}. The only oxygen site with full occupation is that of O1, *i.e.* 24*e*, since this atom takes part of vanadium coordination sphere. The rest of oxygens are situated at two crystallographically different 96*k* sites with 75 % of occupancy providing 25 % of oxygen vacancies.

This structural determination provided probable positions for all cations and anions in addition to the Zhou's research [25], which offered only positions for V^{5+}. Both approaches assume that V^{5+} ions occupy fully 4*a* and partially 32*f* with the difference in V^{5+}-coordination at 4*a*. Namely, according to Zhou's type I, V^{5+} is surrounded by 4 oxygens in tetrahedral environment and 4 vacancies also tetrahedrally arranged. In this research, we wanted to preserve the initial idea that δ-Bi_2O_3 demonstrates such great conductivity not just because of increased number of oxygen vacancies but because of Bi^{3+} roll in this process. In that way, all assumed vacancies in the here proposed modulated structure are located around Bi^{3+}. The unusual bismuth coordination confirms its adjustability to any environment as a consequence of stereochemically active lone electron pare and thus the polarizability of Bi^{3+}.

The thermal behavior of obtained δ*-Bi_2O_3 phases, given in the form of cyclic DTA curves, is presented in Fig. 4. All five phases show very similar behavior on heating. With slight difference in temperatures, three endothermic peaks are visible and could be assigned to δ*-Bi_2O_3 → γ-Bi_2O_3 → δ*-Bi_2O_3 → Bi_2O_3(l) transitions. On cooling, δ*-Bi_2O_3 phases crystallize from the melts and remain stable down to about 530 °C. At this temperature, an

order-disorder transition takes place for all samples but for $Bi_{102}V_6O_{168}$. This is partially in accordance with the XRD findings since the weak XRD reflections, which point out to the existence of a supercell, were the least visible for this sample. In order to clarify this mild contradiction between DTA and XRD analysis, the HRTEM was employed. According to the high-resolution TEM image (Fig. 5a) of $Bi_{102}V_6O_{168}$, the dopant is well integrated into the cubic crystal structure with no evident defects. However, the periodical repeating of the same plane groups (three in a row) in both directions is visible on HRTEM image as well as on SAED pattern (Fig. 5b). The reflections are easily indexed in $Fm\bar{3}m$ space group and 3×3×3 supercell. This means that one order-disorder transition should exist as well for $Bi_{102}V_6O_{168}$, but it was not detected by performed DTA procedure.

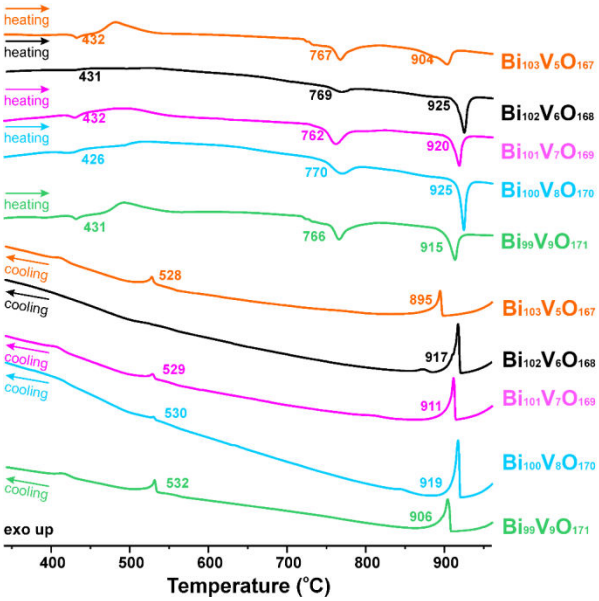

Fig. 4. DTA cyclic curves of single-phase microcrystalline samples. The temperatures (°C) of each phase transition are shown on corresponding curve and are in accordance with the Bi_2O_3–V_2O_5 phase diagram [42].

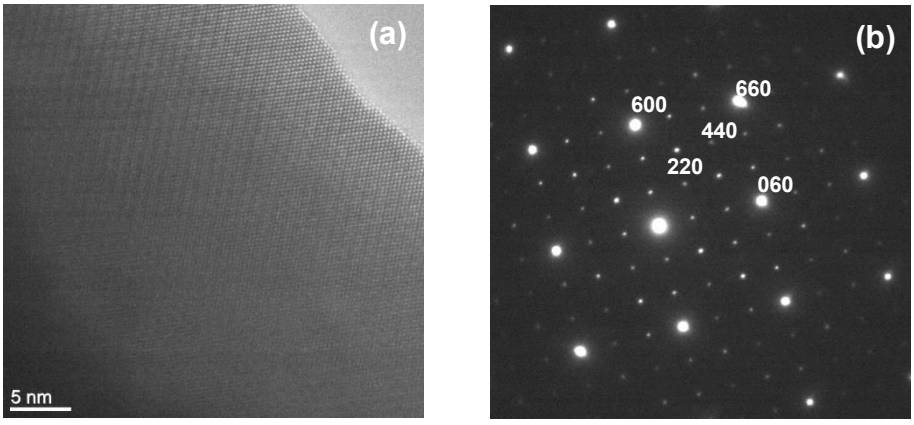

Fig. 5. (a) HRTEM image (b) SAED pattern of $Bi_{102}V_6O_{168}$ grain in [001] zone axis.

The ionic conductivities (Table III) were calculated from the total electrical resistance determined from the impedance spectra (Fig. 6 is an example). It is clear that the sample with the lowest dopant content, *i.e.* $Bi_{103}V_5O_{167}$, demonstrates the highest conductivities at

corresponding temperatures. This can be attributed to the mentioned replacement of trivalent cation (Bi^{3+}) by pentavalent one (V^{5+}) and, as a consequence, to the decrease in number of vacancies. The experiment was performed for 800-750 °C temperature interval since the δ-Bi_2O_3 based phases, which were not previously melted, behaved differently on cooling than the one obtained from the melts. Namely, according to Bi_2O_3–V_2O_5 phase diagram [45], the δ-Bi_2O_3 → γ-Bi_2O_3 transition takes place on cooling at about 750 °C if δ-Bi_2O_3 phase was not previously melted.

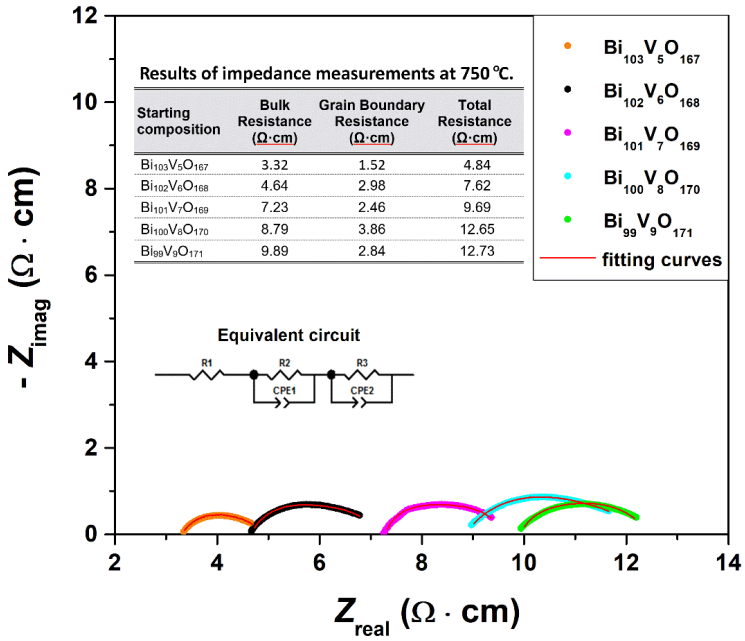

Fig. 6. Impedance spectra of V-doped δ*-Bi_2O_3 phases in form of Nyquist plots at 750 °C. The electrical model in the inset has been used to fit the impedance data.

The Arrhenius plots (Fig. 7), which were extracted from the values of total resistance measured at different temperatures, confirm that the sample with the lowest dopant content is the best conductor, *i.e.* the activation energy (E_a) for $Bi_{103}V_5O_{167}$ is the lowest. This is certainly due to the highest Bi content and mentioned polarizability of Bi^{3+}. However, according to Kuang *et al.* [47] V^{5+}-ion also has an active role in the process of conductivity if the distance between two V^{5+}-ions is larger than 6.7 Å. This could be the reason why E_a of $Bi_{103}V_5O_{167}$ is not significantly higher than that of the undoped δ-Bi_2O_3, which is 0.3 eV [48]. Indeed, according to the here proposed 3×3×3 superstructure the content of V is such that V^{5+}-ions occupy mostly 4*a* site and thus the distance between them is about 11.8 Å. With increase in V content, more of V^{5+}-ions are closer to each other since the content of V exceed 4*a* site and more of V^{5+}-ions are additionally placed at 32*f* since. The distance between V^{5+} at 4*a* and 32*f* is about 6.7 Å and, as a consequence, E_a for other obtained samples are higher. The trend of increasing E_a with V-content increasing is preserved with the exception of $Bi_{102}V_6O_{168}$. This is probably due to experimental error since the standard deviation is quite high for this measurement. If we do not consider the result at 750 °C, activation energy will amount 0.74(3), which is more logical value.

In summary, the $Bi_{103}V_5O_{167}$ conductivity of 0.283 S cm^{-1} at 800 °C is one of the highest among all published V-containing Bi_2O_3 phases [31, 49–52]. This is valid also for δ-Bi_2O_3 type phases doped and double doped with other cations such as Nb and various lanthanides [53–59]. The closest value of conductivity (0.75 S cm^{-1}) was obtained for

$Bi_{12}Tb_3O_{22.5}$ but at 880 °C [1] and for Tm-doped δ-Bi_2O_3 type phases (0.312 – 0.398 S cm^{-1} at 800 °C dependently of Tm content) [21].

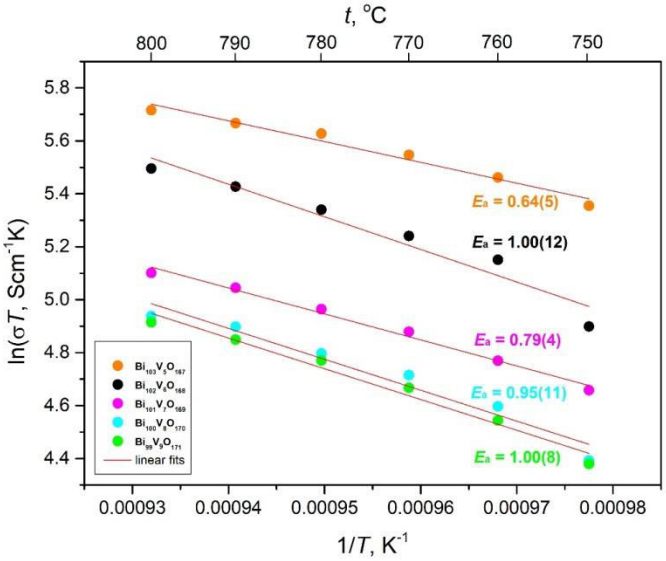

Fig. 7. Arrhenius plots of V-doped δ*-Bi_2O_3 phases.

4. Conclusion

In order to find a minimal V concentration that stabilizes δ-Bi_2O_3 phase, six pseudo-binary Bi_2O_3-V_2O_5 mixtures [3.50 < $x(V_2O_5)$ < 8.50 mol%] were thermally treated at 1000 °C for 1 h. The single phase microcrystalline specimens containing a phase based on simple cubic δ-Bi_2O_3 were obtained if V_2O_5 content was ≥ 4.63 mol%. The crystal structure analysis showed a threefold repeat on a simple cubic sublattice. It means that all obtained phases crystalize in $Fm\bar{3}m$ space group with 3×3×3 supercell. The Rietveld refinement of $Bi_{102}V_6O_{168}$ finally solved issues about this modulated structure. Octahedrally coordinated V^{5+} ions are located at 4*a* with full occupation while eight- and four-coordinated Bi^{3+} fully occupy 24*e* and 48*h*. The only cation site that is shared between V^{5+} and Bi^{3+} is 32*f*. Oxygen vacancies are provided by two crystallographically different 96*k* sites with 75 % of occupancy. Oxygen atoms belonging to the vanadium coordination sphere are located at 24*e* with full occupation. In total, 22% of anionic sites are vacant. The suggested modulated structure was confirmed by DTA and HRTEM/SAED.

The ionic conductivity of phase with the lowest dopant content, *i.e.* $Bi_{103}V_5O_{167}$, amounts 0.283 S cm^{-1} at 800 °C, which is one of the highest conductivities among all published vanadium doped Bi_2O_3 phases. The activation energy for this process is comparable to that of the undoped phase, which is related to the minimal quantity of V. With such high conductivity and low activation energy, we can recommend this material as an electrolyte for SOFCs having operating temperature around 800 °C.

Acknowledgments

The authors acknowledge the financial support of the Ministry of Education, Science and Technological Development of the Republic of Serbia (Grant No. 451-03-68/2020-

14/200135 and 451-03-68/2020-14/200053). The TEM work was conducted in the Centre for Electron Microscopy and Microanalysis (CEMM) at Jožef Stefan Institute, Ljubljana (Slovenia).

5. References

1. P. Shuk, H.-D. Wiemhöfer, U. Guth, W. Göpel, M. Greenblatt, Solid State Ionics 89 (1996) 179.
2. F. Krok, I. Abrahams, W. Wrobel, A. Kozanecka-Szmigiel, J. R. Dygas, Mater. Sci.-Poland 24 (2006) 13.
3. J.-C. Boivin, Int. J. of Inorg. Mater. 3 (2001) 1261.
4. M. Mirković, A. Dosen, S. Erić, M. Stojmenović, B. Matović, A. Rosić, Sci. Sinter. 50 (2018) 95.
5. A. Laarif, F. Theobald, Solid State Ionics 21 (1986) 183.
6. S. C. Singhal, MRS Bull. 25 (2000) 16.
7. B. C. H. Steele, Solid State Ionics 129 (2000) 95.
8. M. Mogensen, N. M. Sammes, G. A. Tompsett, Solid State Ionics 129 (2000) 63.
9. M. Mori, T. Abe, H. Itoh, O. Yamamoto, Y. Takeda, T. Kawahara, Solid State Ionics 74 (1994) 157.
10. O. Yamamoto, Y. Arati, Y. Takeda, N. Imanishi, Y. Mizutani, M. Kawai, Y. Nakamura, Solid State Ionics, 79 (1995) 137.
11. S. Cheng, C. Chatzichristodoulou, M. Søgaard, A. Kaiser, P. Vang Hendriksen,
1. J. Electrochem. Soc. 164 (2017) F1354.
12. E. D. Wachsman, K. T. Lee, Science 334 (2011) 935.
13. L. G. Sillén, Ark. Kemi Mineral. Geol. 12A (1937) 1.
14. G. Gattow, H. Schröder, Z. Anorg. Allg. Chem. 318 (1962) 176.
15. P. W. M. Jacobs, D.A. Mac Donaill, Solid State Ionics 23 (1987) 279.
16. H. A. Harwig, Z. Anorg. Allg. Chem. 444 (1978) 151.
17. B. T. M. Willis, Acta Crystallogr. 18 (1965) 75.
18. P. D. Battle, C. R. A. Catlow, J. Drennan, A. D. Murray, J. Phys. C 16 (1983) 561.
19. M. Yashima, D. Ishimura, Chem. Phys. Lett. 378 (2003) 395.
20. E. M. Levin, R. S. Roth, J. Res. Nat. Bur. Stand. 68A (1964) 189.
21. A. Dapčević, D. Poleti, J. Rogan, A. Radojković, M. Radović, G. Branković, Solid State Ionics 280 (2015) 18.
22. S. Boyapati, E. D. Wachsman, N. Jiang, Solid State Ionics 140 (2001) 149.
23. S. Boyapati, E. D. Wachsman, B. C. Chakoumakos, Solid State Ionics 138 (2001) 293.
24. D. S. Aidhy, S. B. Sinnott, E. D.Wachsman, S. R. Phillpot, J. C. Nino, J. Solid State Chem. 182 (2009) 1222.
25. W. Zhou, J. Solid State Chem. 76 (1988) 290.
26. W. Zhou, J. Solid State Chem. 87 (1990) 44.
27. E. Capoen, M. C. Steil, N. Tancret, G. Nowogrocki, J.C. Boivin, G. Mairesse, R. N. Vannier, M. Anne, O. Isnard, Solid State Ionic 175 (2004) 419.
28. G. Mairesse, P. Roussel, R. N. Vannier, M. Anne, G. Nowogrocki, Solid State Sciences 5 (2003) 861.

29. G. Mairesse, P. Roussel, R. N. Vannier, M. Anne, C. Pirovano, G. Nowogrocki, Solid State Sciences 5 (2003) 851.
30. A. Watanabe, Solid State Ionics 96 (1997) 75.
31. A. Watanabe, J. Solid State Chem. 161 (2001) 410.
32. F. Mauvy, J. C. Launay, J. Darriet, J. Solid State Chem. 178 (2005) 2015.
33. S. Kashida, T. Hori, J. Solid State Chem. 122 (1996) 358.
34. J. Darriet, J. C. Launay, F. J. Zúniga, J. Solid State Chem. 178 (2005) 1753.
35. A. A. Bush, S. Yu. Stefanovich, Yu. V. Titov, Zh. Neorg. Knim, 41 (1996) 1568.
36. G. Pang, S. Feng, Y. Tang, R. Xu, Chem. Mater. 10 (1998) 2446.
37. S. Kashida, T. Hori, K. Nakamura, J. Phys. Soc. Jpn. 63 (1994) 4422.
38. R. G. Garwey: LSUCRIPC, least squares unit-cell refinement with indexing on the personal computer. Powder Diffr. 1 (1986) 114.
39. ICSD-Inorganic Crystal Structure Database, FIZ Karlsruhe and National Institute of Standards (NIST), version 1.9.4, 2014-1.
40. J. Rodriguez-Carvajal, FULLPROF: A program for Rietveld refinement and pattern matching analysis, Version 1.9c, (2001) France.
41. T. Roisnel, J. Rodriguez-Carvajal, WINPLOTR: A graphic tool for powder diffraction, (2005) France.
42. J. N. Stojanović, S. V. Smiljanić, S. R. Grujić, P. J. Vulić, S. D. Matijašević, J. D. Nikolić, V. Savić, Sci. Sinter. 51 (2019) 389.
43. J. Maletaškić, M. Čebela, M. Pekajski Đorđević, D. Kozlenko, S. Kichanov, M. Mitrić, B. Matović, Sci. Sinter. 51 (2019) 71.
44. A. S. Bondarenko, G. A. Ragoisha, in "Progress in Chemometrics Research", Ed. A. L.Pomerantsev, Nova Science Publishers, New York, 2005, p. 89–102.
45. Yu. F. Kargin, V. Yu. Voevodski, Zh. Neorg. Knim 42 (1997) 1547.
46. R. D. Shannon, Acta Crystallogr. A32 (1976) 751.
47. X. Kuang, J. L. Payne, M. R. Johnson, I. Radosavljevic Evans, Angew. Chem. Int. 51 (2012) 690.
48. H. A. Harwig, A. G. Gerards, J. Solid State Chem. 26 (1978) 265.
49. S. Giraud, S. Obbade, E. Suard, H. Steinfink, J.-P. Wignacourt, Solid State Sciences 5 (2003) 335.
50. P. Roussel, S. Giraud, E. Suard, J.-P. Wignacourt, H. Steinfink, Solid State Sciences 4 (2002) 1143.
51. N. Portefaix, P. Conflant, J.C. Boivin, J.P. Wignacourt, M. Drache, J. Solid State Chem. 134 (1997) 219.
52. A. Diktanaitė, G. Gaidamavičienė, E. Kazakevičius, A. Kežionis, A. Žalga, Thermochim. Acta 685 (2020) 178511.
53. H. T. Cahen, T. G. M. Van Den Belt, J. H. W. De Wit, G. H. J. Broers, Solid State Ionics 1 (1980) 411.
54. H. Iwahara, T. Esaka, T. Sato, T. Takahashi, J. Solid State Chem. 39 (1981) 173.
55. M. J. Verkerk, G. M. H. Van De Velde, A. J. Burggraaf, R. B. Helmholdt, J. Phys. Chem. Solids 43 (1982) 1129.
56. J. Berezovsky, H. K. Liu, S. X. Dou, Solid State Ionics 66 (1993) 201.
57. S. Durmuş, V. Corumlu, T. Cifci, I. Ermis, M. Ari, Ceram. Int. 39 (2013) 5241.
58. A. Watanabe, M. Sekita, Solid State Ionics 176 (2005) 2429.
59. T. Esaka, H. Iwahara, J. Appl. Electrochem. 15 (1985) 447.

Сажетак: *У овом раду испитивана је могућност стабилизовања кисеоничних јонских проводника у систему Bi_2O_3-V_2O_5. Шест псеудо-бинарних смеша Bi_2O_3-V_2O_5 [3.50 < $x(V_2O_5)$ < 8.50 mol%] је термички третирано на 1000 °C током 1 h. Добијени узорци су окарактерисани техникама XRD, HRTEM/SAED, DTA и EIS. У случајевима када је садржај V_2O_5 био ≥ 4.63 mol%, реакцијом између α Bi_2O_3 and V_2O_5 настали су микрокристални једнофазни узорци који су садржали фазу базирану на δ-Bi_2O_3. Добијене фазе показују главне рефлексије које одговарају простом кубном δ-Bi_2O_3 (просторна група Fm-3m), али је Ритвелдовим утачњавањем утврђено да долази до стварања 3×3×3 суперћелије. У овој ћелији јони V^{5+} су октаедарски координисани на положају 4a и делимично заузимају положај 32f. Јони Bi^{3+} допуњавају положај 32f и у потпуности заузимају положаје 24e и 48h. 22 % анјонских места је упражњено. Јонска проводност фазе са најмањим садржајем допанта, $Bi_{103}V_5O_{167}$, износи 0,283 S cm^{-1} на 800 °C уз енергију активације од 0,64(5) eV, што је поредиво са недопираним δ-Bi_2O_3, који је најбржи познати јонски проводник.*

Кључне речи*: Bi_2O_3, V_2O_5, јонски проводници, суперћелија.*